Quantitative analysis of the time course of Aβ oligomerization and subsequent growth steps using tetramethylrhodamine-labeled Aβ

Kanchan Garai and Carl Frieden[1]

Department of Biochemistry and Molecular Biophysics, Washington University School of Medicine, St. Louis, MO 63110

Contributed by Carl Frieden, December 27, 2012 (sent for review November 13, 2012)

Although amyloid β (Aβ) is a critical player in the pathology of Alzheimer's disease, there is currently little Information on the rate and extent of formation of oligomers that lead to the presence of Aβ fibrils observed in amyloid plaques. Here we describe a unique method to monitor the full time course of Aβ aggregation. In this method, Aβ is labeled with tetramethylrhodamine at a lysine residue on the N-terminal end. During aggregation, the fluorescence is quenched in a time-dependent manner in three distinct phases: an early oligomerization phase, an intermediate phase, and a growth phase. The oligomerization phase can be characterized as a monomer-dimer-trimer process for which we have determined the rate and equilibrium constants. The rate constants differ markedly between $Aβ_{1–42}$ and $Aβ_{1–40}$, with $Aβ_{1–42}$ showing a greater oligomerization propensity. The intermediate phase reflects slow clustering and reorganization of the oligomers, whereas the growth phase ultimately results in the formation of fibrillar material. The data are consistent with a conformational change being an important rate-limiting step in the overall aggregation process. The rates of all phases are highly sensitive to temperature and pH, with the pH-dependent data indicating important roles for lysine and histidine residues. From the temperature-dependent data, activation energies of oligomerization and fibrillization are estimated to be 5.5 and 12.1 kCal/mol, respectively. The methodologies presented here are simple and can be applied to other amyloidogenic peptides or proteins.

oligomer formation | fluorescence quenching | kinetics of aggregation | nucleation

Alzheimer's disease (AD), the most prevalent form of neurodegenerative diseases, is characterized by deposition of senile plaques in the brain. These plaques contain aggregates of the amyloid β (Aβ) peptides $Aβ_{1–42}$ and $Aβ_{1–40}$. In vitro, both peptides self-assemble into soluble oligomers and insoluble fibrils in a time-dependent manner. There has been extensive structure–function characterization of the in vitro aggregation process using a large number of available methods (1). The most widely used method follows changes in the fluorescence of Thioflavin T (ThT). This dye is particularly useful because of the large fluorescence increase observed during the final phase of aggregation coincident with the formation of β-strand structure. This assay, however, does not report on intermediates in the aggregation process and therefore cannot detect soluble oligomers that lack well-defined β-strand structure. It is critical to understand the nature of these small oligomers, because recent experiments suggest that they may be the major cytotoxic species for AD (2–5).

Data in the literature present a highly complex picture of the oligomer formation, starting from dimers to spherical oligomers and linear protofibrils comprised of a large number of monomers. Biophysical characterization of the low-molecular-weight oligomers, however, has been difficult because of their small size and metastable nature. Bitan et al. (3), for example, characterized the low-molecular-weight oligomers of $Aβ_{1–40}$ and $Aβ_{1–42}$ by stabilizing them using covalent cross-linking. More recently, mass spectrometry coupled with ion mobility spectrometry (IM-MS) experiments have provided information regarding the size and shape of the low-molecular-weight oligomeric forms of Aβ and other amyloidoic proteins (6, 7). A variety of biophysical methods have been used to study the oligomers extensively (2, 7–14).

Despite such studies, the ability to measure the rates of formation of the oligomers remains difficult. Recently, Lee et al. (15) reported a method suitable for monitoring the full time course of aggregation showing distinct phases corresponding to oligomerization and fibrillization using Cys-Cys-Aβ and FlAsH dye binding to tetracysteine motifs arising from self-association of Aβ. A quantitative characterization of the monomer-oligomer process, however, is still lacking. Here we report a fluorescent method that allows characterization of the full time course of aggregation including the early events—specifically those involved in the formation of low-molecular-weight oligomers—as well as the fibrillization process. The method uses tetramethylrhodamine (TMR) covalently attached to an N-terminal lysine residue of Aβ. The basis for this assay is fluorescence self-quenching as discussed by Zhuang et al. (16) and used by Chattopadhyay et al. (17) to measure the kinetics of conformational fluctuations in an unfolded protein. Our assay, applied to both $Aβ_{1–40}$ and $Aβ_{1–42}$, allows us to determine rate constants of the early steps of the monomer-oligomer process. In this paper, we compare this assay with those using ThT or circular dichroism (CD) and discuss their similarities and differences. Finally, we use this assay to determine the time course of Aβ self-assembly as a function of temperature and pH.

Results

Time Course of Fluorescence and Circular Dichroism Changes Using TMR-Labeled Aβ. Fig. 1 compares the time course of the TMR fluorescence and the CD data measured at 216 nm of TMR-labeled $Aβ_{1–42}$. The experiments were performed at room temperature in 20 mM phosphate buffer, at pH 7.5, containing 15 mM NaCl with continuous stirring. The TMR fluorescence decreases in at least three distinct phases: a fast small decrease in fluorescence completed within 30–45 min, which, as described below, we term the oligomerization phase; followed by a longer phase of ∼500 min, termed the intermediate (or lag) phase, during which there is only a small change in fluorescence; and finally, a rapid and large decrease in fluorescence, which we call the growth phase. Conversely, the CD data show a long lag followed by a rapid increase in β-structure formation. In this experiment, the $Aβ_{1–42}$ concentration was 2 μM, and the data were normalized for comparison. From the raw TMR data, some fluorescence remains at long times. Assuming this represents monomer, the final $Aβ_{1–42}$ concentration can be calculated to be 0.35 μM, ∼15% of the starting material.

Author contributions: K.G. and C.F. designed research; K.G. performed research; K.G. and C.F. analyzed data; and K.G. and C.F. wrote the paper.

The authors declare no conflict of interest.

[1]To whom correspondence should be addressed. E-mail: frieden@biochem.wustl.edu.

This article contains supporting information online at www.pnas.org/lookup/suppl/doi:10.1073/pnas.1222478110/-/DCSupplemental.

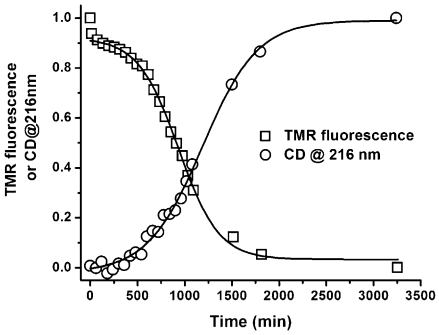

Fig. 1. Normalized time course of changes in TMR fluorescence (□) and in CD (○). TMR-Aβ_{1-42} (2 μM) was prepared in 20 mM phosphate buffer at pH 7.5 containing 15 mM NaCl, 0.1 mM EDTA, and 0.5 mM βMe. TMR fluorescence was monitored at 600 nm with excitation at 520 nm. The CD signal was monitored at 216 nm. Both measurements were performed on the same sample. Solid lines are sigmoidal fits to the data. The data were normalized by setting the fluorescence at zero time to 1 and that at long times to zero.

Although the CD data are consistent with a classical nucleation-elongation model, the TMR data refute this model, clearly indicating substantial self-association before the growth phase. The growth phase of the TMR fluorescence data is similar to the CD change, although the half-time ($t_{1/2}$) of the growth phase observed from TMR fluorescence (~910 min) is somewhat less than that observed from the CD data (~1,210 min).

Time Course of Aggregation Using Unlabeled and TMR-Labeled Aβ. We then compared the TMR-Aβ assay to the ThT assay of unlabeled Aβ under a variety of conditions. Fig. 2 *A–C* compares the time course of aggregation between TMR-labeled Aβ_{1-42} and unlabeled Aβ_{1-42} at two different temperatures (25 and 50 °C; Fig. 2 *A* and *B*) and two different pH values (pH 7.5 and 6.5; Fig. 2 *A* and *C*). Under all conditions, the fluorescence of TMR-Aβ_{1-42} (red curves) shows the same three distinct phases discussed in Fig. 1, whereas those of the ThT assay (blue curves) show only a lag and a growth phase. Again, the TMR assay shows that the classical nucleation-elongation model is not an appropriate description of the process. In all cases, the growth phase of the TMR-Aβ (red curves) assay is similar to that of unlabeled Aβ measured by ThT fluorescence (blue curves), indicating minimal interference of the attached TMR on aggregation of Aβ. However, the half-time ($t_{1/2}$) of the growth phase, as measured by TMR fluorescence, is shorter than that measured by ThT fluorescence, possibly indicating unstructured aggregation before appearance of fibrils as will be discussed later. It is evident from Fig. 2 that the time course of Aβ aggregation is highly sensitive to changes in temperature and pH. We address this issue in more detail in later sections.

In the case of TMR-Aβ_{1-40}, the loss of fluorescence in the first phase was small (Fig. 2*D*, red curves) for reasons discussed later. It should be noted that the ThT fluorescence decreases at long times as a result of precipitation of large fibrils.

Effect of TMR Labeling on the Morphology of Aβ Fibrils. Fig. 3 shows negative-stain EM images of samples prepared under identical conditions. It may be seen that the EM images of the TMR-Aβ_{1-42} and TMR-Aβ_{1-40} fibrils are similar to those of unlabeled Aβ_{1-42} and Aβ_{1-40}. All of the peptides formed amyloid fibrils that are similar in width (~6 nm) and length (>100 nm). Overall, our data indicate that TMR labeling does not significantly affect Aβ fibril morphology.

Oligomerization Phase. Figs. 1 and 2 show a rapid decrease in TMR fluorescence in the first 30–45 min, during which time the ThT fluorescence did not change. To examine the meaning of this phase, we prepared a stock solution of monomeric TMR-labeled Aβ in 4 M GdnCl as described in *Materials and Methods*. Fig. 4 shows the time-dependent changes of TMR fluorescence following dilution of this material into 20 mM phosphate buffer at pH 7.5 and 25 °C. The final GdnCl concentration in all solutions was 0.16 M. Fig. 4*A* shows that the change of TMR fluorescence is negligible at an Aβ_{1-42} concentration of 0.5 μM. At higher concentrations, the TMR fluorescence changes in a time-dependent manner over 30 min. We interpret the quenching of TMR fluorescence to be a result of self-association

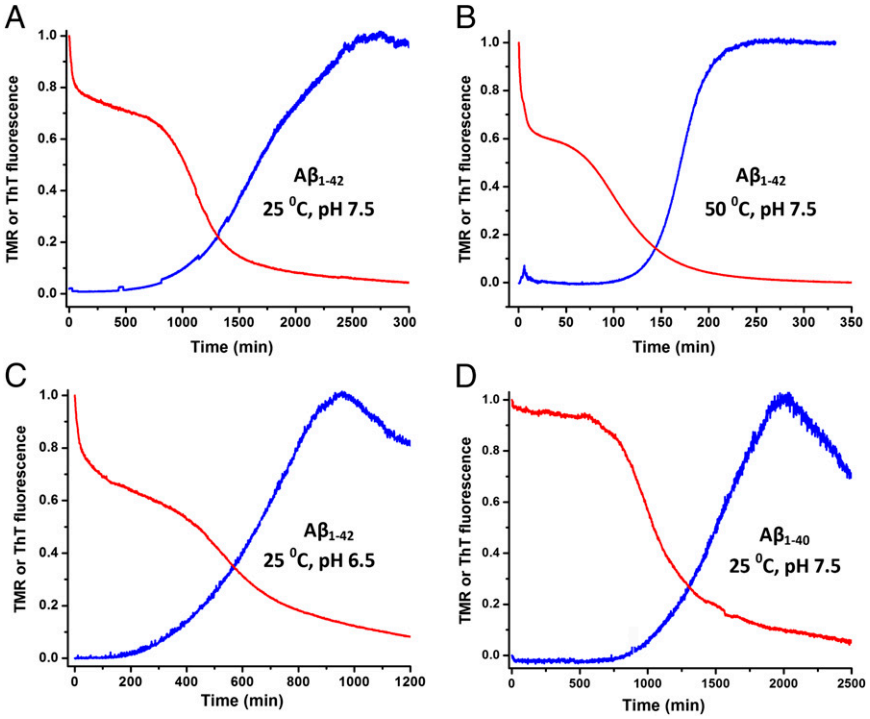

Fig. 2. Time courses using TMR (red) or ThT fluorescence (blue) under various conditions. *A–C* use unlabeled or TMR-labeled Aβ_{1-42} at (*A*) 25 °C, pH 7.5; (*B*) 50 °C, pH 7.5; and (*C*) 25 °C, pH 6.5. (*D*) Time course of unlabeled and TMR-labeled Aβ_{1-40} at 25 °C, pH 7.5. All buffers contained 150 mM NaCl, 1 mM EDTA, and 5 mM βMe. The unlabeled Aβ samples contained 2 μM ThT and were monitored at an emission wavelength 470 nm with excitation at 438 nm. The data were normalized for comparative purposes.

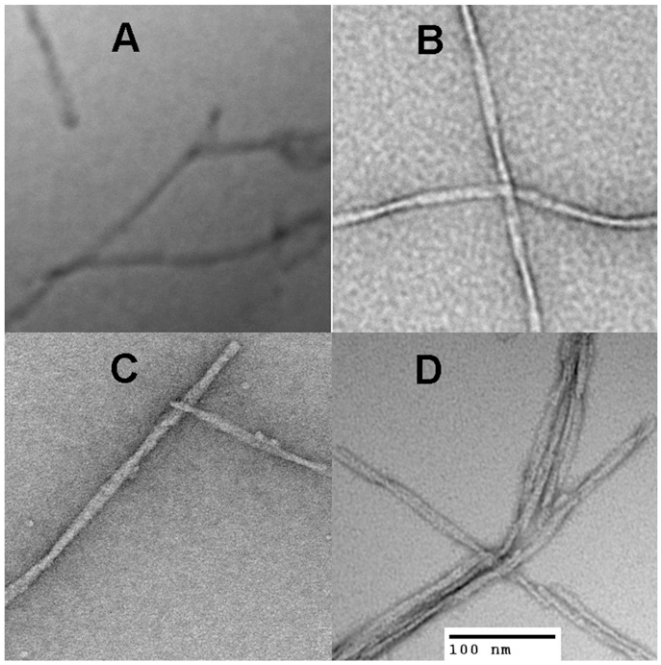

Fig. 3. Negative stain electron microscopy images of Aβ fibrils collected from the endpoints of the experiments shown in Fig. 2 prepared in pH 7.5 and incubated at 25 °C. (*A*) unlabeled $A\beta_{1-42}$, (*B*) unlabeled $A\beta_{1-40}$, (*C*) TMR-$A\beta_{1-42}$, and (*D*) TMR-$A\beta_{1-40}$.

to form low-molecular-weight oligomers. A two-exponential equation is required to fit these data, indicating the formation of more than one species from the monomer. The kinetic data can be globally fit (solid red lines) assuming a simple monomer-dimer-trimer model as shown in Scheme 1. When similar experiments are performed with $A\beta_{1-40}$ (Fig. 4*B*), the fluorescence change is much smaller and the rates are slower. The individual rate constants obtained for the monomer-dimer-trimer scheme for both $A\beta_{1-42}$ and $A\beta_{1-40}$ are summarized in Table 1.

Intermediate (Lag) Phase. Figs. 1 and 2 show that, after the first rapid phase reflecting oligomerization, there is a phase during which there is only a slight decrease in fluorescence, suggesting little incorporation of monomer in this phase. The fluorescence change in this phase is larger for $A\beta_{1-42}$ than for $A\beta_{1-40}$. In either case, this phase may reflect either the clustering of the oligomeric species and/or the reorganization of the oligomeric species already present. In any case, these clusters, containing disordered monomers of Aβ, are not recognized by ThT. The data also suggest that these clusters do not fluoresce as brightly as the monomer.

$$m_1 \underset{k_{-12}}{\overset{k_{+12}}{\rightleftharpoons}} m_2 \underset{k_{-23}}{\overset{k_{+23}}{\rightleftharpoons}} m_3$$

Scheme 1. Monomer-dimer-trimer process of Aβ oligomerization.

Growth Phase. The final time-dependent fluorescence change is large as measured by changes in both TMR-Aβ and ThT fluorescence (Fig. 2 *A–D*). This phase is also correlated with appearance of the β-structure as measured by CD (Fig. 1). As will be discussed below, the rate of this phase, as measured by the TMR assay, appears somewhat faster than that measured by the ThT assay, although the length of time before this phase is almost the same for these two assays. In this and all other experiments, the rate of this phase is possibly enhanced by fragmentation of the fibril caused by stirring the solution.

pH Dependence of the Phases. The data in Fig. 2 indicated a strong pH dependence of the three phases that describe the aggregation process. Fig. S1 *A* and *B* shows kinetic data for the oligomerization phase and the full time course of TMR-$A\beta_{1-42}$ as a function of pH. The data clearly show that the phases are highly sensitive to pH. Fig. 5*A* shows the plot of extent of oligomerization (estimated in the first 20 min) derived from the data presented in Fig. S1*A*. There are clear changes in oligomerization behavior around pH 6.5 and pH 11.0. Fig. 5*B* shows the plot of $1/t_{1/2}$ of the growth phase as a function of pH derived from the data presented in Fig. S1*B*. Clearly, the overall rates are faster at low pH, with a midpoint between pH 6.5 and pH 7.0.

Temperature Dependence of the Phases. Fig. 2 *A* and *B* indicates that the rate of oligomerization, the extent of the intermediate phase, and the rate of the growth phase are all highly sensitive to temperature. We addressed this issue by performing experiments over a range of solution temperatures (from ~3 °C to ~75 °C). The temperature-dependent kinetic data of TMR-$A\beta_{1-42}$ are shown in Fig. S2 *A* and *B*. Fig. 6 *A* and *B* shows Arrhenius plots (squares) of the temperature dependence data. The solid lines represent fits of the data to the Arrhenius equation as described by Eq. **1a** (*Materials and Methods*). It is clear from the figures that the data do not conform to the Arrhenius equation over the full temperature range but rather deviate at temperatures >50 °C. Fitting the data below 50 °C yields the values of activation energies (E_a) of the oligomerization and growth phases to be 5.5 and 12 kCal/mol, respectively. Deviations from the Arrhenius equation at high temperatures may arise as a consequence of reduced hydrophobic interactions between the peptides under these conditions or from a change in the mechanism of oligomerization.

Discussion

We developed a unique fluorescent assay to monitor the full time course of fibril formation using TMR covalently attached to the Aβ peptide. The basis for this assay is fluorescence self-quenching (17). Although there are many assays that are used to monitor different aspects of amyloid aggregation, the major

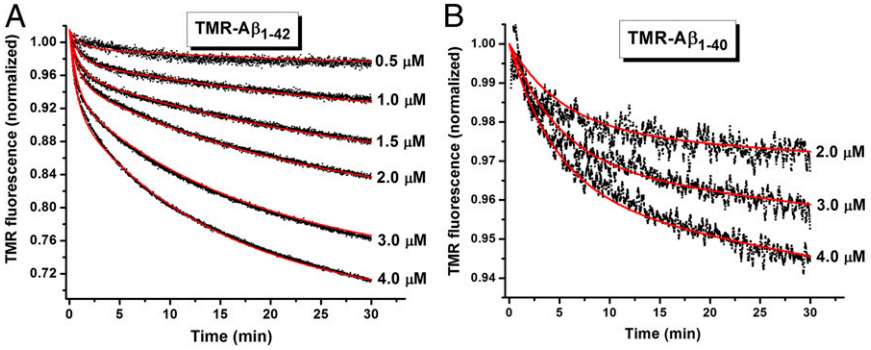

Fig. 4. Oligomerization of TMR-labeled Aβ. Time course of fluorescence change following dilution of a 100 μM stock solution containing monomeric (*A*) TMR-$A\beta_{1-42}$ or (*B*) TMR-$A\beta_{1-40}$, prepared in 4 M GdnCl, to final concentrations from 0.5 to 4.0 μM in 20 mM phosphate buffer at pH 7.5 containing 1 mM EDTA and 5 mM βMe. The black dots represent data, and the red lines are global fit of the data using a monomer-dimer-trimer model as described in Scheme 1. The rate constants obtained are summarized in Table 1. In all of the samples, the final concentration of GdnCl is 0.16 M. All experiments were performed at 25 °C without stirring.

Table 1. Rate constants for the monomer-dimer-trimer process of Aβ oligomerization

Sample	k_{+12} ($M^{-1}s^{-1}$) × 10^2	k_{-12} (s^{-1}) × 10^{-3}	k_{+23} ($M^{-1}s^{-1}$)	k_{-23} (s^{-1}) × 10^{-3}	K_{12}^{-1} (M) × 10^{-6}	K_{23}^{-1} (M) × 10^{-6}
TMR-$A\beta_{1-42}$	9.9 ± 1.9	12.7 ± 3.0	38 ± 5	0.3 ± 0.1	12.8	7.9
TMR-$A\beta_{1-40}$	0.5 ± 0.05	2.7 ± 0.3	20 ± 10	0*	54.0	ND

ND, not determined.
*Value of this parameter was too small; hence, it was set equal to 0.

advantage of the TMR assay is the ability to follow, by a convenient fluorescent method, the early formation of oligomers. In this assay, the oligomerization phase is clearly separated from the growth phase by an intermediate or lag phase, enabling quantitative analysis of the data.

TMR Assay and the ThT Assay May Be Complementary. ThT fluorescence has been the most widely used method to detect or monitor amyloid aggregation. ThT fluorescence, however, is not suitable for mechanistic studies primarily because it does not report on early steps in the aggregation process. The fact that TMR fluorescence is sensitive to early oligomeric steps enables us to monitor and quantitate the earliest phase of aggregation. Conversely, the ThT assay does report on the formation of structured fibrils, so it can be complementary to data obtained with the TMR assay. Careful examination of the data in Fig. 2, for example, shows that there are differences in the growth phase, suggesting that the TMR assay is measuring large oligomers that do not necessarily have the canonical β-strand structure typical of fibrils.

Interpretation of the Oligomerization and Intermediate Phases. Data in the literature present a highly complex picture of Aβ oligomers starting from dimers and proceeding to large-sized spherical oligomers or the protofibrils with little quantitative characterization (2–6, 8–12, 14). Thus, it has been impossible to establish a complete kinetic scheme of oligomerization.

The TMR data presented in Figs. 1, 2, 4, 5, and 6 support the concept of spontaneous oligomer formation during the early phase of aggregation. We show that this phase can be simply described by a monomer-dimer-trimer process with different rate and equilibrium constants for dimer and trimer formation. Attempts to fit the data to an isodesmic model were not successful. Our data for both $A\beta_{1-40}$ and $A\beta_{1-42}$ collected over a range of concentrations are consistent with this model (Fig. 4). It is also well known that $A\beta_{1-42}$ aggregates more readily than $A\beta_{1-40}$, and the data of Table 1 show that $A\beta_{1-42}$ monomers self-associate to dimers and trimers more readily than do monomers of $A\beta_{1-40}$ (3). The rate constants for association to dimer or trimer are, however, well below what would be expected for a diffusion controlled process. This suggests that the formation of oligomers may be a rare event, perhaps due to only rare forms forming stable dimers. This interpretation is consistent with the view that the monomers of Aβ exist in multiple conformations and that the predominant or the lowest energy conformers are not suitable for self-association (18).

From the rate constants, we can calculate apparent equilibrium constants. For the monomer-dimer process, this value is 12.8 μM for $A\beta_{1-42}$ and 54 μM for $A\beta_{1-40}$ (Table 1). Thus, it is not surprising that oligomers of $A\beta_{1-40}$ hardly form at concentrations of 2–4 μM, as shown in Fig. 4. Using the rate constants shown in Table 1, we can simulate the appearance of the oligomers. Fig. 7 shows these simulations for $A\beta_{1-42}$ and $A\beta_{1-40}$ using a starting concentration of 2 μM. It is clear that both dimers and trimers of $A\beta_{1-42}$ form faster and to a greater extent than do oligomers of $A\beta_{1-40}$. It may be recalled here that the oligomers, especially the dimers of $A\beta_{1-42}$, have been detected in the cortices of AD patients' brains, although the total $A\beta_{1-42}$ concentration in the brain is only a few nanomolar (19). How the oligomers of $A\beta_{1-42}$ form at such low concentrations is not clear, but the presence of lipids, membranes, and macromolecular crowding in vivo may catalyze such processes (20, 21). Additionally, physiological temperature (37 °C) and low pH, especially that found in the intracellular lysosomal compartments, can have catalytic effects on the oligomerization of $A\beta_{1-42}$ (22).

It is of interest that at 10- to 100-fold higher Aβ concentrations and using chemical cross-linking or ion mobility MS (IM-MS), investigators have detected the presence of dimer, trimer, tetramer, and higher oligomers of both $A\beta_{1-40}$ and $A\beta_{1-42}$ (3, 6).

As mentioned earlier, during the intermediate phase, there is very little fluorescence change, yet the aggregation process still continues and probably represents the formation of large clusters of the dimeric and trimeric or higher oligomers. There is very little fluorescence change during this time, because the concentration of highly fluorescent monomers is not being significantly depleted.

Growth Phase. Our data show that the $t_{1/2}$ of the growth phase of Aβ aggregation is highly dependent on temperature (Figs. 2 and 6) but relatively independent of the initial Aβ concentration (Fig. S3). Such a result could arise from a concentration-independent step, such as a conformational change, being rate limiting. We suggest that this step occurs within the phase we characterized as the intermediate phase that follows the initial oligomerization process. Our data, and that from numerous other groups, have shown the presence of metastable oligomers of $n \geq 2$ before fibrillization of $A\beta_{1-42}$ (3, 4, 10, 15), clearly refuting the homogeneous nucleation model. Several authors have suggested that conformational conversion of the monomers occurs within the

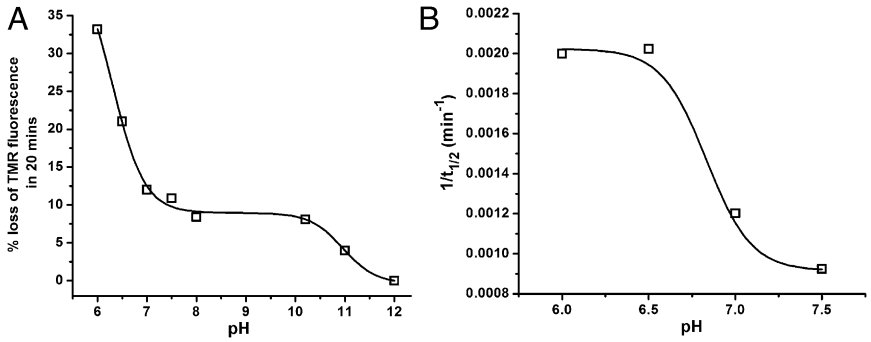

Fig. 5. pH dependence of oligomerization and fibrillization. (*A*) Extent of loss of TMR fluorescence in 20 min following dilution of a 100 μM stock solution of monomeric TMR-$A\beta_{1-42}$ to 2.0 μM and (*B*) the inverse of half-time ($t_{1/2}$) of the growth phase of TMR-labeled $A\beta_{1-42}$ at different pH values. Empty squares represent data, and the solid lines represent sigmoidal fit of the data. The final buffer concentration was 20 mM phosphate at all pH values.

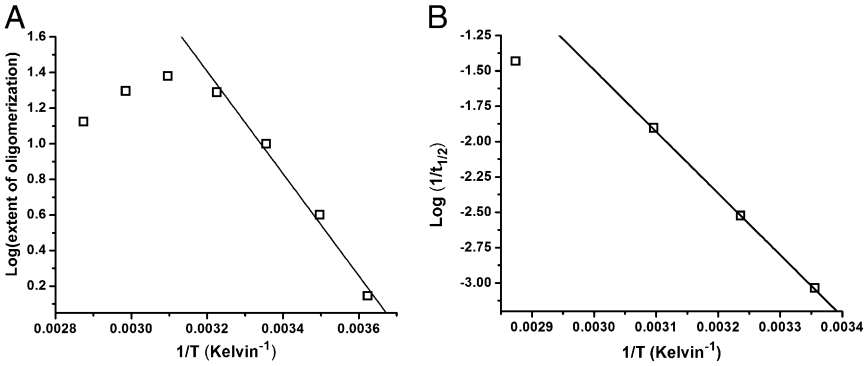

Fig. 6. Temperature dependence of oligomerization and fibrillization. Arrhenius plots of (*A*) the extent of loss of TMR fluorescence in 20 min following dilution of a 100 μM stock solution of monomeric TMR-Aβ_{1-42} to 2.0 μM and (*B*) the half-time of the growth phase of TMR-labeled Aβ_{1-42} into 20 mM phosphate, pH 7.5 buffer at different temperatures. Empty squares represent data, and the solid lines represent fit of the data to Arrhenius equation as described in Eq. **1a**.

liquid-like oligomers (15, 23). Our data agree with this mechanism and show that this step is pH and temperature dependent.

Activation Barrier of Oligomerization and Fibrillization. The activation barrier between the monomers and the oligomers is 5.5 kCal/mol and that between the monomers and fibrils is 12.1 kCal/mol. The high activation barrier separating the fibrils from other species can explain the long intermediate phase observed before the growth phase. We note here that, using a similar approach, the E_a of fibrillization for Aβ_{1-40} at pH 3.0 and pH 7.4 was earlier reported to be 23 and 74 kCal/mol, respectively (24, 25). However, to our knowledge, the E_a of oligomerization for any amyloidic protein has never been reported.

Importance of the Lysine and Histidine Residues in Oligomer Formation. Fig. 5*A* shows the oligomerization process to be highly sensitive to pH, with little self-association above pH 11.0, almost pH-independent behavior between pH 7.5 and pH 10.2, and increasingly faster oligomerization below pH 7.5. Additionally, the growth phase is also quite sensitive to pH, with significantly lower $t_{1/2}$ values for the growth phase below pH 7.0 (Fig. 5*B*). Because lysine and histidine side chains have pK_a values of 10.5 and 6.5, respectively, it is likely that these residues play important roles in both the oligomerization and growth phases. The large changes below pH 7.5 suggest an important role for histidine, even though the 3 histidine residues are clustered within the first 14 residues and are sequentially distant from residues proposed to be involved in a turn motif (Asp23-Lys28) (26).

Overall Mechanism. Fig. 8 shows a schematic view of the aggregation process based on the data that are presented here. The red circles are disordered monomers labeled with TMR, whereas the black circles are those monomers in which the TMR fluorescence has been quenched. The step from position A to B represents the formation of dimers and trimers observed in the oligomerization phase. The step from position B to C reflects the clustering of these oligomers to form larger, perhaps micelle-like, species composed of disordered monomers. At point C, a conformational change occurs, allowing the rapid formation of fibrils with the canonical β-strand structure. Some monomers may persist even after complete fibrillization.

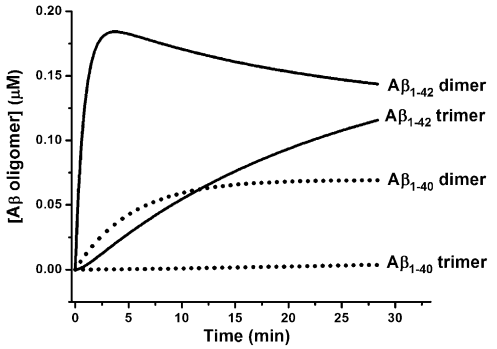

Fig. 7. Simulation of time course of oligomerization by Aβ_{1-40} and Aβ_{1-42}. Time course of dimer and trimer formation for Aβ_{1-42} (solid lines) and Aβ_{1-40} (dotted lines) starting from 2 μM monomer. The curves were simulated by Kintek explorer (28) using the rate constants listed in Table 1.

Conclusion

In summary, we developed a unique method that allows investigation of the early steps in the formation of Aβ fibrils. Using this assay, we determined the rate constants for the formation of dimers and trimers that are the earliest events in the formation of fibrillar structures. Our data are consistent with a conformational change of monomers within an intermediate oligomeric form being the rate-determining step of fibrillization of Aβ. We speculate that our method would be applicable to study other amyloidic proteins such as α-synuclein and polyglutamine repeat proteins.

Materials and Methods

Preparation of TMR-Labeled Aβ. Unlabeled and TMR-labeled Aβ peptides were chemically synthesized and purchased from Keck Foundation (Yale University). The peptides were purified by reverse-phase LC using a C18 column in water/acetonitrile media. The purified peptides were lyophilized and resuspended in 6 M GdnCl. The Aβ peptides were further purified by size exclusion chromatography using a Superdex peptide column (GE Healthcare) in 4 M GdnCl and 20 mM phosphate, pH 7.5, or 3 mM NaOH. The predominant fraction was selected for subsequent experiments.

Measurement of Aβ Oligomerization. Appropriate volumes of TMR-Aβ_{1-42} or TMR-Aβ_{1-40} prepared in 4 M GdnCl and 20 mM phosphate, pH 7.5, were diluted from a 100-μM stock solution to final peptide concentrations ranging

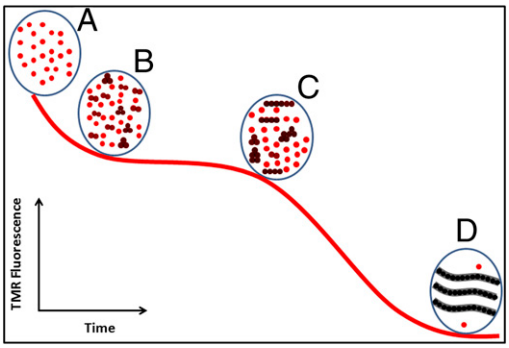

Fig. 8. Schematic view of aggregation based on time course of TMR fluorescence. The red curve is a typical fluorescence time course of TMR-Aβ. (*A*) Monomeric ensemble at $t = 0$, (*B*) small oligomers predominantly dimers and trimers formed during the oligomerization phase, (*C*) small oligomers cluster to larger oligomers during the intermediate or lag phase, and (*D*) β-structured fibrillar aggregates are formed and the solution is monomer depleted.

from 0.5 to 4 μM into 20 mM phosphate buffer, pH 7.5, at 25 °C. The final concentration of GdnCl was adjusted to 160 mM in all samples. The fluorescence of TMR was monitored as a function of time in an Alphascan fluorometer (PTI), with excitation and emission monochromators set to 520 and 600 nm, respectively. The monochromator positions were chosen slightly away from the excitation and emission maxima of TMR (550 and 575 nm, respectively) to avoid inner filter effect by the dye at micromolar concentrations.

Fluorescence Time Course Measurements. A 20-μM stock solution of unlabeled Aβ or TMR-labeled Aβ prepared in 3 mM NaOH was diluted to 4.0 μM final concentration in 20 mM phosphate buffer, pH 7.4, containing 150 mM NaCl, 1 mM EDTA, and 5 mM β-mercaptoethanol (βME) and incubated in a clean glass test tube with continuous stirring in a temperature-controlled cuvette holder. The unlabeled Aβ samples contained 2.0 μM ThT. Aggregation of unlabeled and TMR-labeled Aβ samples was monitored continuously using ThT (λ_{ex} = 438 nm, λ_{em} = 480 nm) or TMR (λ_{ex} = 520 nm, λ_{em} = 600 nm). To increase the rate of fibrillization, all samples were stirred using a stir bar. Because variations of stirring speed can alter the aggregation kinetics, the temperature- and pH-dependent experiments reported here were performed at the same stirring speeds.

CD Measurements. The CD measurements were performed on 2.0 μM TMR-$A\beta_{1-42}$ in 20 mM phosphate buffer containing 15 mM NaCl, 0.1 mM EDTA, and 0.5 mM βME in a Jasco 715 spectropolarimeter. The samples, prepared in a 1 × 1-cm quartz cuvette, were continuously stirred at room temperature between measurements.

Electron Microscopy of Aβ Aggregates. Unlabeled $A\beta_{1-42}$ and $A\beta_{1-40}$ and TMR-labeled $A\beta_{1-42}$ and $A\beta_{1-40}$, prepared in 20 mM phosphate buffer at pH 7.5 containing 150 mM NaCl, 1 mM EDTA, and 5 mM β ME, were stored at room temperature for 2 d in glass test tubes with continuous stirring. The aggregates were then resuspended in the solution by a brief vortexing. Each sample of 10 μL volume was incubated on a Formvar carbon-coated 200 mesh copper grid (Electron Microscopy Sciences) for 1 min. The grid was washed twice in buffer, followed by two washes in distilled water. Finally, the grid was negatively stained in 0.5% uranyl acetate for 1 min and then dried in a desicator overnight at room temperature. The images were collected in a JEOL 100CX transmission electron microscope equipped with an AMT digital camera.

Data Analysis. ***Fitting the Kinetic Data.*** The kinetic data of the oligomerization of TMR-$A\beta_{1-42}$ and TMR-$A\beta_{1-40}$ were fit globally to the monomer-dimer-trimer model shown in Scheme 1 using a similar approach previously applied to a protein that was described by a monomer-dimer-tetramer process (27). The time-dependent TMR-Aβ fluorescence, $F(t)$, is expressed as $F(t) = c[m_1(t) + e_2m_2(t) + e_3m_3(t)]$, where c is a normalization constant, m_1, m_2, and m_3 are concentrations of monomers, dimers and trimers respectively, and e_2 and e_3 are the average relative (compared with the monomers) brightness values of the dimers and the trimers respectively. Experiments were simulated starting with monomers of Aβ at multiple concentrations ranging from 0.5 to 4.0 μM. The kinetic data at all of the concentrations were fit globally by Kintek Explorer (Kintek Corp.) (28) to obtain the four rate constants and two brightness values. The values of e_2 and e_3 were allowed to float in the fitting process and then held constant for fitting the rate constants (Table 1).

Estimation of Activation Energy from Temperature-Dependent Kinetic Data. Temperature dependence of the rate (r) of a chemical reaction is commonly described by the following Arrhenius equation:

$$r = A\exp\left(-\frac{E_a}{k_B T}\right), \quad [1]$$

where A is the preexponential factor that takes into account a number of factors such as the frequency of collision between and the orientation of the reacting particles, E_a is the activation energy, k_B is the Boltzmann constant, and T is the absolute temperature of the solution. Alternatively Eq. **1** can be expressed as

$$\log r = \log A - \frac{E_a}{k_B}\left(\frac{1}{T}\right). \quad [1a]$$

For a single rate-limited thermally activated process, the log$r$ vs. 1/T plot gives a straight line. The activation energy, E_a can be determined from the slope of the straight line.

The rate of oligomerization is calculated as the extent of change of TMR fluorescence in the initial 20 min. The rate of fibrillization is assumed to be proportional to the inverse of the half-time ($1/t_{1/2}$) of aggregation. $t_{1/2}$ values were calculated from the quenching that occurs after the oligomerization phase. The E_a of oligomerization or fibrillization is calculated from the slope of the linear region of the log$r$ vs. 1/T plot.

ACKNOWLEDGMENTS. We thank Dr. Rohit Pappu and Dr. Scott Crick for discussions and critical reading of the manuscript. This work was supported in part by a grant from the American Health Assistance Foundation (to C.F.).

1. Morris AM, Watzky MA, Finke RG (2009) Protein aggregation kinetics, mechanism, and curve-fitting: A review of the literature. *Biochim Biophys Acta* 1794(3): 375–397.
2. Lashuel HA, Hartley D, Petre BM, Walz T, Lansbury PT, Jr. (2002) Neurodegenerative disease: Amyloid pores from pathogenic mutations. *Nature* 418(6895):291.
3. Bitan G, et al. (2003) Amyloid beta -protein (Abeta) assembly: Abeta 40 and Abeta 42 oligomerize through distinct pathways. *Proc Natl Acad Sci USA* 100(1):330–335.
4. Klein WL, Stine WB, Jr., Teplow DB (2004) Small assemblies of unmodified amyloid beta-protein are the proximate neurotoxin in Alzheimer's disease. *Neurobiol Aging* 25(5):569–580.
5. Jin M, et al. (2011) Soluble amyloid beta-protein dimers isolated from Alzheimer cortex directly induce Tau hyperphosphorylation and neuritic degeneration. *Proc Natl Acad Sci USA* 108(14):5819–5824.
6. Bernstein SL, et al. (2009) Amyloid-β protein oligomerization and the importance of tetramers and dodecamers in the aetiology of Alzheimer's disease. *Nat Chem* 1(4): 326–331.
7. Smith DP, Radford SE, Ashcroft AE (2010) Elongated oligomers in beta2-microglobulin amyloid assembly revealed by ion mobility spectrometry-mass spectrometry. *Proc Natl Acad Sci USA* 107(15):6794–6798.
8. Lomakin A, Benedek GB, Teplow DB (1999) Monitoring protein assembly using quasielastic light scattering spectroscopy. *Methods Enzymol* 309:429–459.
9. Parbhu A, Lin H, Thimm J, Lal R (2002) Imaging real-time aggregation of amyloid beta protein (1-42) by atomic force microscopy. *Peptides* 23(7):1265–1270.
10. Garai K, Sahoo B, Kaushalya SK, Desai R, Maiti S (2007) Zinc lowers amyloid-beta toxicity by selectively precipitating aggregation intermediates. *Biochemistry* 46(37): 10655–10663.
11. Carulla N, et al. (2009) Experimental characterization of disordered and ordered aggregates populated during the process of amyloid fibril formation. *Proc Natl Acad Sci USA* 106(19):7828–7833.
12. Hashimoto T, Adams KW, Fan Z, McLean PJ, Hyman BT (2011) Characterization of oligomer formation of amyloid-beta peptide using a split-luciferase complementation assay. *J Biol Chem* 286(31):27081–27091.
13. Krishnan R, et al. (2012) Conserved features of intermediates in amyloid assembly determine their benign or toxic states. *Proc Natl Acad Sci USA* 109(28):11172–11177.
14. Fawzi NL, Ying J, Torchia DA, Clore GM (2010) Kinetics of amyloid beta monomer-to-oligomer exchange by NMR relaxation. *J Am Chem Soc* 132(29):9948–9951.
15. Lee J, Culyba EK, Powers ET, Kelly JW (2011) Amyloid-β forms fibrils by nucleated conformational conversion of oligomers. *Nat Chem Biol* 7(9):602–609.
16. Zhuang X, et al. (2000) Fluorescence quenching: A tool for single-molecule protein-folding study. *Proc Natl Acad Sci USA* 97(26):14241–14244.
17. Chattopadhyay K, Elson EL, Frieden C (2005) The kinetics of conformational fluctuations in an unfolded protein measured by fluorescence methods. *Proc Natl Acad Sci USA* 102(7):2385–2389.
18. Straub JE, Thirumalai D (2011) Toward a molecular theory of early and late events in monomer to amyloid fibril formation. *Annu Rev Phys Chem* 62:437–463.
19. Shankar GM, et al. (2008) Amyloid-beta protein dimers isolated directly from Alzheimer's brains impair synaptic plasticity and memory. *Nat Med* 14(8):837–842.
20. Davis CH, Berkowitz ML (2009) Interaction between amyloid-beta (1-42) peptide and phospholipid bilayers: A molecular dynamics study. *Biophys J* 96(3):785–797.
21. Munishkina LA, Cooper EM, Uversky VN, Fink AL (2004) The effect of macromolecular crowding on protein aggregation and amyloid fibril formation. *J Mol Recognit* 17(5): 456–464.
22. Hu X, et al. (2009) Amyloid seeds formed by cellular uptake, concentration, and aggregation of the amyloid-beta peptide. *Proc Natl Acad Sci USA* 106(48):20324–20329.
23. Auer S, Ricchiuto P, Kashchiev D (2012) Two-step nucleation of amyloid fibrils: Omnipresent or not? *J Mol Biol* 422(5):723–730.
24. Kusumoto Y, Lomakin A, Teplow DB, Benedek GB (1998) Temperature dependence of amyloid beta-protein fibrillization. *Proc Natl Acad Sci USA* 95(21):12277–12282.
25. Sabaté R, Gallardo M, Estelrich J (2005) Temperature dependence of the nucleation constant rate in beta amyloid fibrillogenesis. *Int J Biol Macromol* 35(1-2):9–13.
26. Sciarretta KL, Gordon DJ, Petkova AT, Tycko R, Meredith SC (2005) Abeta40-Lactam (D23/K28) models a conformation highly favorable for nucleation of amyloid. *Biochemistry* 44(16):6003–6014.
27. Garai K, Frieden C (2010) The association–dissociation behavior of the ApoE proteins: Kinetic and equilibrium studies. *Biochemistry* 49(44):9533–9541.
28. Johnson KA, Simpson ZB, Blom T (2009) Global kinetic explorer: A new computer program for dynamic simulation and fitting of kinetic data. *Anal Biochem* 387(1): 20–29.